Quantitative biomechanical imaging via magnetic resonance elastography

Olivier Beuf, Philippe Garteiser, Kevin Tse-Ve-Koon, Jonathan Vappou

7

Quantitative biomechanical imaging via magnetic resonance elastography

Olivier BEUF[1], Philippe GARTEISER[2], Kevin TSE VE KOON[1] and Jonathan VAPPOU[3]

[1] *CREATIS, CNRS, Inserm, INSA Lyon, Université Claude Bernard Lyon 1, Lyon, France*
[2] *Centre of recherche sur l'inflammation, Inserm, Paris, France*
[3] *ICUBE, CNRS, Université of Strasbourg, Strasbourg, France*

7.1. Fundamentals of magnetic resonance elastography

7.1.1. *Introduction*

Many pathologies affect the tissue structure and composition at different levels, including cellular modifications and the interactions betweencells and their close surroundings, from the extracellular matrix up to the entire organ. Since the tissue structure and its composition determine how these tissues deform in response to an applied force, there is correlation between the mechanical properties and the pathologic tissue alterations.

Due to this fact, the measurement of mechanical tissue properties or « elastography » has been proposed as a quantitative marker of pathological or healthy conditions. Several development efforts have been dedicated to imaging methods that would be capable of measuring the mechanical properties in a clinical setting.

MRI challenges,
coordinated by Hélène RATINEY and Olivier BEUF.

Historically, ultrasound elastography has been the first instance of virtual palpation. Magnetic resonance imaging has been later adopted as an imaging tool to develop magnetic resonance elastography (MRE). Regardless of the underlying imaging method, all elastography approaches are based on three aspects: the application of a static or dynamic constraint, the measurement of the induced deformation and the reconstruction of mechanical properties. In the case of MRE, these elements consist of the generation and propagation of a shear wave, a phase-contrast MRI sequence, and a quantitative reconstruction starting from the estimation of the shear modulus.

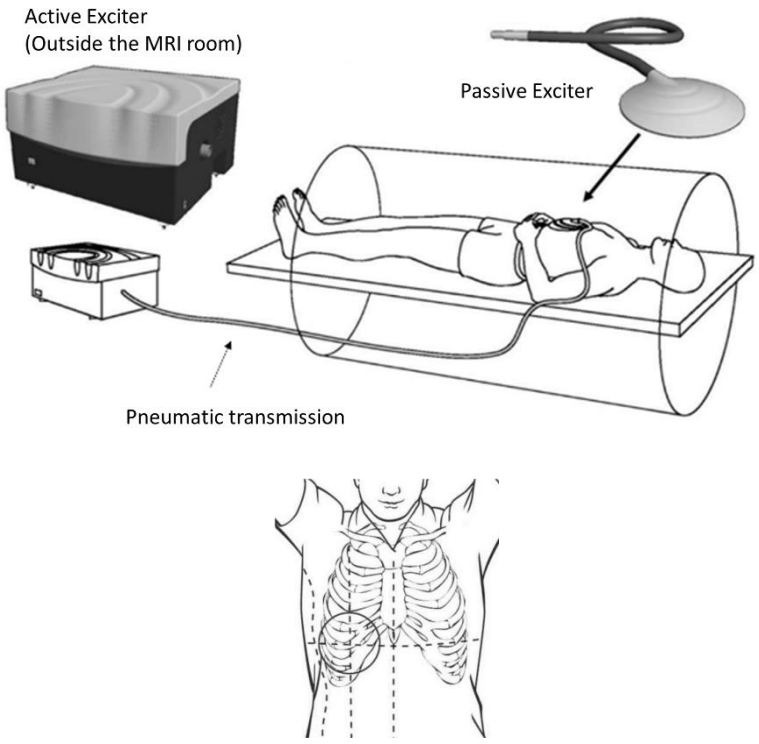

Figure 7.1. *Schematics of a pneumatic transducer employed in a clinical setting. The passive transducer is placed upon the thorax to transmit shear waves to the liver. Image from Resoundant (Rochester, MN, USA)*

Frequencies in the order of 50 Hz are typically used in clinics or even higher frequencies, in particular in preclinical scanners, where higher spatial resolutions are required. Several driver technologies are employed to produce shear waves in the region of interest. The most common approach in clinical settings is pneumatic excitation: a

loudspeaker located outside the MRI room delivers acoustic vibration via a semi-rigid tube to a passive transducer made of a chamber with a membrane that vibrates in contact with the patient's skin (Venkatesh *et al.* 2013) as illustrated in figure 7.1. Mechanical excitation can also be generated by an electromechanical or piezoelectric transducer and can be transmitted as a rigid motion to the MRI room, directly delivered to the actuator (Tse *et al.* 2009), or obtained from the rotation of an axis with an eccentric mass at its end in contact with the patient (Runge *et al.* 2019).

In such practical conditions, which are the most common ones, the displacement induced in tissues by the external transducer can be considered to be well represented by a harmonic plane shear wave. This hypothesis enables applying well-established wave propagation equations to estimate local mechanical properties. The equation of a propagating wave in a linear viscoelastic medium is given by:

$$-\rho\omega^2 u = \mu\Delta u + i\omega\eta.\Delta u \qquad [7.1]$$

where ρ is the tissue density, ω is the angular frequency of the wave, and u is the displacement field (and Δ is its Laplacian). Here, the mechanical properties are composed of a real part μ corresponding to the elasticity of the tissue and of an imaginary part $\omega\eta$ corresponding to its viscosity that together can be represented as a complex shear modulus G:

$$G = \mu + i\omega\eta \qquad [7.2]$$

The real part of G is the storage modulus, sometimes denoted as G', and corresponds to the elasticity of the tissue, whereas the imaginary part, or loss modulus G'', is related to its viscosity. The magnitude of G and the damping ratio $G''/2G'$, derived from the representation of the complex value G in polar coordinates are sometimes employed. In this way, we obtain the fundamental equation that relates the displacement induced by the wave to the mechanical properties of the medium in which it propagates:

$$-\rho\omega^2 u = G.\Delta u \qquad [7.3]$$

To visualize the waves generated via the different vibration devices mentioned above, motion-sensitive imaging sequences have to be used. For this purpose, encoding gradients are added to standard sequences such as gradient echo or spin echo sequences. The employed encoding gradients are designed to create a phase change in the signal that is proportional to the displacement (Lewa 1991). In order to solve equation [7.3], instantaneous tissue displacement has to be detected. This is achieved by temporally synchronizing the encoding gradients ($\vec{G}_{MEG}$ in the equation [7.4]) with the mechanical vibration and repeating the measurement for different phase offsets between the encoding gradient and the mechanical vibration. The obtained phase can be expressed in terms of the time profile of the gradients and the tissue displacement at a point $\vec{r}$ in the image:

$$\phi = \gamma \int_{t_0}^{t_0+\tau_G} \vec{G}_{MEG}(t).\vec{u}(\vec{r}.t)dt \quad [7.4]$$

In practice, most often, gradients (typically with a sinusoidal or trapezoidal shape) that oscillate at the same frequency as the mechanical wave are used. Tissue displacement can also be described as sinusoidal motion whose frequency is imposed by the transducer and whose amplitude and phase vary within the sample. When required, the different spatial components of displacement can be estimated by consecutively encoding the motion with gradients oriented along the three spatial directions.

Once the phase images are obtained, phase unwrapping followed by a conversion from radians to micrometers is performed to obtain the displacement field $\vec{u}$. The compression displacement component is then removed (using one of the several available methods), to obtain the complete shear displacement field (typically as amplitude and phase data in the acquired image domain). The latter is then used to perform a local inversion of the equation [7.3] thus leading to an estimation of *G* over the entire image or on an area of the image where both wave propagation and sufficient signal-to-noise ratio are obtained.

7.1.2. *MRE signal encoding*

If we consider a (plane) shear wave that propagates in the y-direction with displacement motion along the z-direction, the displacement field can be expressed as:

$$\vec{u}(\vec{r},t) = Asin(\omega t - k.y + \theta_0)\overrightarrow{u_z} \quad [7.5]$$

A represents the amplitude of this wave, ω is its frequency, *k* is the wave vector, oriented here along the *y*-direction, and θ_0 is the initial phase of the wave which for now we consider equal to zero. Equation [7.4] shows that in order to encode this wave displacement into the phase of the MRI signal, the gradient $\vec{G}_{MEG}(t)$ has to have at least one component parallel to the direction of tissue displacement (*z* in equation [7.5]). Ideally, to maximize the encoding, $\vec{G}_{MEG}(t)$ is chosen such that:

$$\vec{G}_{MEG}(t) = G_0(t)\vec{u}_z \quad [7.6]$$

where $G_0(t)$ is a periodic function (often with the same period as the wave). Figures 7.2A, 7.2B, and 7.2C illustrate the phase encoding in a relatively simple case of a plane wave generated by a vibrating plate with a frequency of 50 Hz and amplitude of 25 µm described by equation [7.5] and a trapezoidal gradient with the same frequency of 50 Hz and an amplitude of 40 mT/m.

Figure 7.2B shows the displacement obtained at four separate points along the direction of propagation as well as the phase variation (according to equation [7.4])

when the motion encoding gradient is applied for one period. Figure 7.2C represents the final phase value depending on the position along the direction of propagation. As we can see, the phase provides an image of the displacement field. Other images at different instants of the wave propagation are required; this is achieved by repeating the acquisition with a delay between the motion and the application of the encoding gradient. Usually, at least four different sequential acquisitions are performed.

By observing the obtained encoded phase in figure 7.2C, it can be noticed that its absolute value is greater than π. In MRI, the signal's phase is bounded between $-\pi$ and π and this means that the acquired phase image will exhibit phase wraps, which can be easily unwrapped in the present example. However, phase continuity between the different acquisitions must be ensured as well, and in the case of more complex or noisy displacement fields, the phase unwrapping step can be quite difficult.

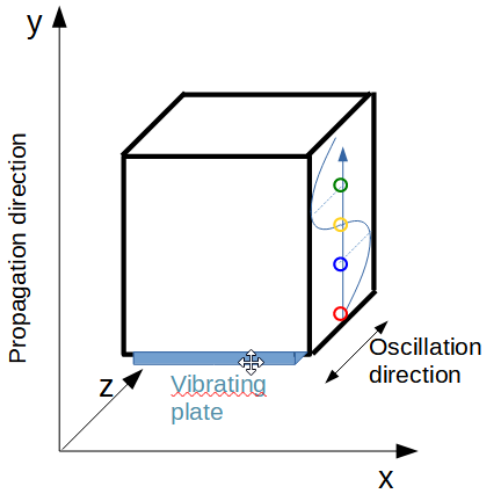

Figure 7.2A. *Schematics illustrating a device for generating shear waves within a phantom*

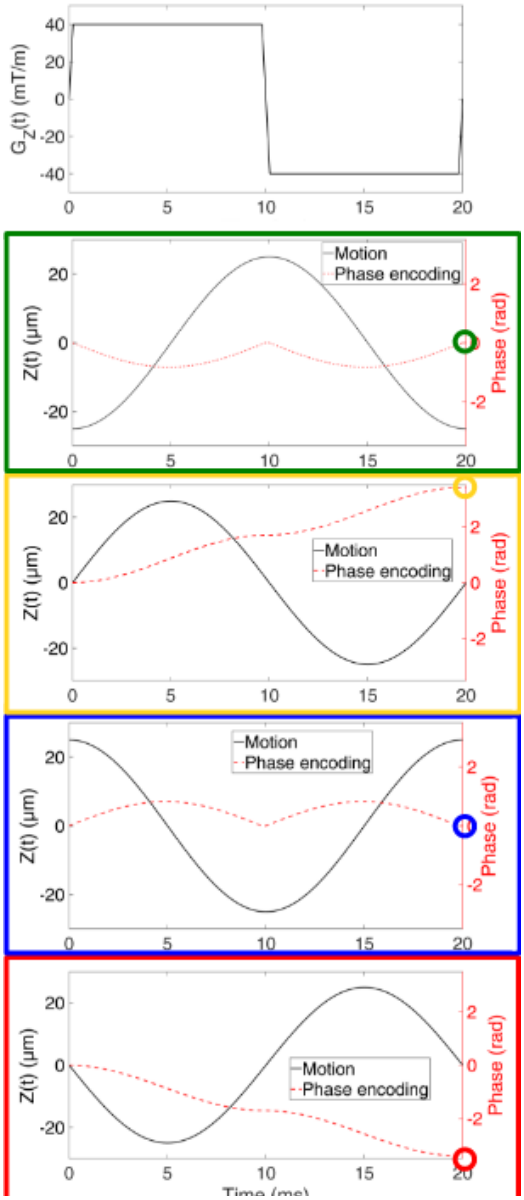

Figure 7.2B. *Motion-encoding gradient (40-mT/m amplitude, 50-Hz frequency) as a function of time, wave (25-µm amplitude and 50-Hz frequency) and phase encoding obtained at 4 equidistant points along the propagation direction during one period.*

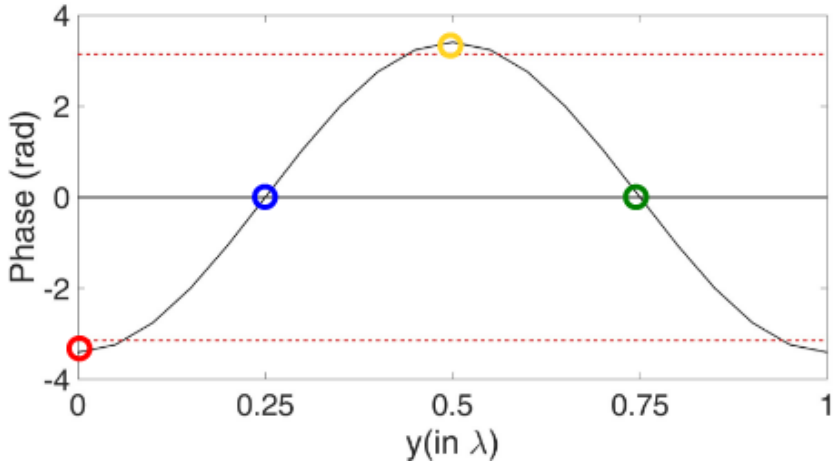

Figure 7.2C. *Phase accumulated after one period at different points along the direction of propagation*

However, the phase of the acquired MRI signal is affected by other physical phenomena that are most of the time static, i.e. constant over time. The most common effect is related to the non-uniformities of the static magnetic field B_0, which translates into a static phase ϕ_s in the acquired images. In order to remove these undesirable effects in MRE, two acquisitions are performed with opposite polarities of the motion-encoding gradients, and the phase signal of interest is retrieved by subtracting the phase images of the two acquisitions. However, since phase images can exhibit different wraps that are not

necessarily well-localized, the phase related to the wave is typically extracted from complex images:

$$\begin{matrix} \phi_{acq1} = \phi_s + \phi_{wave} \\ \phi_{acq2} = \phi_s - \phi_{wave} \end{matrix} \Longrightarrow \quad \phi_{wave} = \frac{1}{2} Arg\left(\frac{e^{i\phi_{acq1}}}{e^{i\phi_{acq2}}}\right) \qquad [7.7]$$

Phase encoding by means of encoding gradients can be added to any kind of MRI sequence. Such gradients are executed after the excitation pulse and before the signal readout gradients, which, as a consequence, increases the echo time. Figure 7.3 represents the case of a gradient echo sequence where motion encoding is performed along the slice direction. Encoding the motion along the other directions is possible as well; displacement fields are commonly acquired in a sequential way along the three orthogonal spatial directions in advanced scans, or even along oblique directions by exploiting the simultaneous application of several gradient directions in order to maximize the effective gradient amplitude. The sequence chronogram in figure 7.3 additionally shows that motion is triggered before the encoding gradients are applied, such that a stationary state of the shear wave is achieved. In some cases, motion is continuously induced, but this requires choosing a TR of the sequence equal to an integer number of motion periods and ensuring the absence of any time drift between the different clocks intervening in a scan (the MRI system clock and vibration device). Accumulation of small delays over several consecutive TRs yields increasingly negative impact over the scan's duration. In order to probe different instants of the wave propagation, a phase offset φ is introduced between the wave and the motion-encoding gradient. Four acquisitions (corresponding to four different values of φ) are usually performed with a constant phase offset over the interval $[0, 2\pi[$, referred to as different phase steps.

The employed frequency of the shear wave is chosen depending on the targeted organ or tissue and on the achievable spatial resolution. Since the wave attenuation increases with increasing frequencies, it is important to choose an appropriate frequency that enables sufficient penetration into the investigated region. Thus, in most clinical MRI scans, the employed frequencies vary between 20 Hz and 200 Hz. The lower frequency boundary is related to the corresponding wavelength. Although a local wavelength measurement is sought (from which to extract the shear speed or shear modulus), it is necessary that the reconstruction step be performed with wavelengths shorter than the size of the targeted organ. Because of this, small-animal applications employ higher frequencies, varying from 200 Hz to approximately 1 kHz.

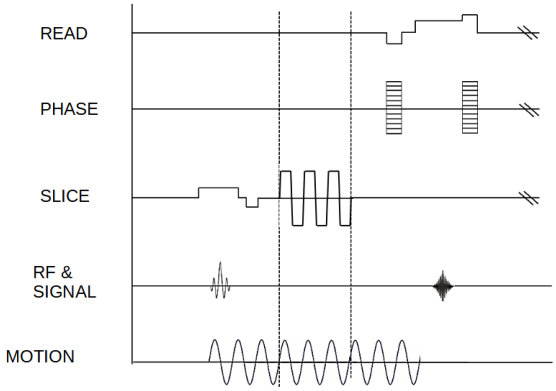

Figure 7.3. *Chronogram of a magnetic resonance elastography sequence based on a gradient echo sequence and an encoding gradient with a duration of three periods along the slice direction*

One last aspect to be taken into account is related to the acquisition matrix in the slice plane. The resulting image should provide a visualization of the wave propagating inside the region of interest, which defines the maximum pixel size in the image plane. On the other hand, the minimum size is imposed by the resulting signal-to-noise ratio (SNR) of the image. A rule of thumb consists in choosing a pixel size such that one wavelength corresponds to about ten pixels while ensuring an SNR greater than 10.

7.1.3. *MRE data reconstruction*

7.1.3.1. *Fundamentals*

Once the displacement field has been encoded into the phase of the MRI signal, the last step is the reconstruction of the mechanical properties. Overall, the various reconstruction methods can be classified into three categories:

1) Local Frequency Estimation methods (LFE). These methods are based on the estimation of spatial frequencies in the wave image, leading to a mapping of the wavelength and thus of the local elasticity. This reconstruction method is employed in approved clinical MRE products and we will describe its principle in detail below;

2) direct inversion methods where the wave equation is inverted are also common and widely used by several research groups. In a purely elastic linear medium, the wave propagation equation [7.1] can be written as:

$$\mu = -\rho\omega^2 \frac{u_i}{\Delta u_i} \quad [7.8]$$

It is thus possible to determine the shear modulus μ by discretizing the above equation. This method, apparently simple, carries however a major disadvantage of being sensitive to noise. We shall see how some conditioning steps such as frequency filtering can significantly improve the robustness of this method;

3) iterative methods: such methods exploit the simulation of displacement fields u_{sim} via direct approaches, for example using finite difference or finite elements. The goal of these methods is to minimize the error between a simulated displacement field u_{sim} and the experimentally measured displacement field u_{exp} (Van Houten *et al.* 1999). Such methods can potentially be powerful as they are capable of extracting the parameters of rather complex models, such as those describing tissue anisotropy, yet they are demanding in terms of computation time.

7.1.3.2. *Pre-processing/conditioning*

Before any inversion algorithm is applied, the first step is to unwrap the phase. The latter is obtained as the arctangent of the ratio between the imaginary part and the real part of the MRI signal, hence it is confined between -π and π. From a physical point of view, there is no reason for the phase to be restricted only to this range and an unwrapping step is often required to retrieve the actual phase. A second step that is widely employed in MRE, including in clinical MRE, consists in filtering based on the temporal Fourier transform (TFT). Applying the TFT is much more than a simple pre-processing step since it leads to direct implications regarding the MRI scan: for example, the N phase steps required for the TFT (typically, $N = 4$) usually imply N different acquisitions and a scan time multiplied by the same factor. For each voxel of the region of interest, TFT is applied to the N measurements, thereby selecting the displacement occurring at the frequency of mechanical excitation while filtering out the other frequency components. This step significantly improves the robustness of the reconstruction.

7.1.3.3. *LFE method: local frequency estimation*

The LFE method is rather complex and our goal here is to illustrate its main aspects. The reader can find detailed explanations in (Manduca *et al.* 2003) as well as in the original article by Knutsson (Knutsson *et al.* 1994) about radar signals which is the foundation for the LFE method in MRE. This method is based on processing steps following a spatial Fourier transform of the wave image. Clearly, spatial frequencies ν (and thus, indirectly, shear wavelengths λ from $\lambda = 1/\nu$) are located in the Fourier space, although without any information on their localization in space. The LFE method enables localizing the spatial frequencies of the Fourier domain in space. For this purpose, it can be shown that the local spatial frequency ν of a signal S can be found by applying lognormal filters R_i and R_j with central frequencies ν_i and ν_j, respectively:

$$\nu = \sqrt{\nu_i \nu_j} Re\left(\frac{r_j \times S}{r_i \times S}\right) \quad [7.9]$$

with r_i and r_j the inverse Fourier transforms of R_i and R_j, respectively. In summary, the LFE algorithm is composed of the following steps:

– Spatial FT of the wave image, displaying the spatial frequency peaks (corresponding to the different wavelengths and thus to elasticity in the image) in the Fourier domain;

– Filtering via pairs of lognormal filters with central frequencies chosen *a priori*;

– Calculation of the ratio between the filtered signals, providing the radial spatial frequency;

– Combination of radial and directional filters to extend the method to a 2D image.

Once these operations have been performed, a map of spatial frequencies $\nu(x,y) = 1/\lambda(x,y)$ is obtained, and hence the shear modulus $\mu(x,y)$ is retrieved with the hypothesis of a purely elastic and incompressible medium via $\mu = \rho.\lambda^2.f^2$, where f is the excitation frequency. Figure 7.4 represents the three steps required to perform an MRE acquisition.

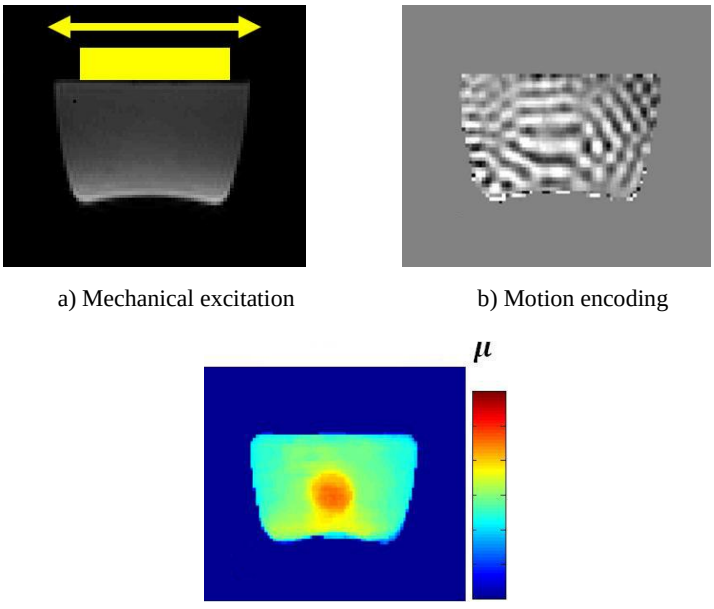

a) Mechanical excitation b) Motion encoding

c) Reconstruction

Figure 7.4. *Illustration of the three steps of an MRE acquisition. a) Generation and transmission of a shear wave in the region of interest, b) visualization of the motion on the phase images of an MRE scan, and c) mapping of the mechanical properties by*

means of reconstruction algorithms. Data obtained in a gel made of 2.5 % gelatine with a stiffer inclusion (4 % gelatine).

7.2. MRE sequences

The way to encode the MRE signal has evolved significantly since the first sequence was proposed (Muthupillai *et al.* 1995). Each modification has sought to perform faster scans, increase the amount of acquired information or decrease the echo time to increase the SNR. Some of such sequences are non-exhaustively described in this section.

7.2.1. *Fractional encoding*

One of the characteristic MRE limitations is related to the duration of the motion-encoding gradients. Since they are applied after the excitation pulse of the imaging sequence, their duration leads to an increase in the echo time causing a loss of signal. This is further reinforced at lower mechanical frequencies. The goal of fractional encoding is to remove this undesired coupling between the applied mechanical frequency and the available signal at the price of reduced sensitivity to motion.

The idea is based on the fact that, according to equation [7.4], it is possible to obtain a non-zero phase accumulation even when the gradient shape is different to the case illustrated in figure 7.2B. In practice, encoding gradients are executed with a frequency higher than the mechanical frequency. This enables a decreased echo time, thanks to the shorter duration of the motion-encoding gradients, and, hence, a gain in signal. Such a strategy can become advantageous in particular in organs such as the liver, where some pathologies are characterized by a strong loss of signal. On the other hand, the difference between the mechanical frequency and the encoding gradient frequency leads to a reduced accumulation of phase, all the more so as a smaller fraction of the mechanical vibration cycle is exploited for the encoding. The ratio q between the duration of the encoding τ_G and the period of the mechanical oscillation T (or, equivalently, between the mechanical frequency and the encoding frequency), $q = \frac{\tau_G}{T} = \frac{\omega}{\omega_G}$, represents then a characteristic variable in the sequence. By integrating equation [7.4], in which the gradient shape is replaced by a sinusoidal signal with a pulsation ω_G (period T_G) and an amplitude G_{MEG}, the accumulated phase ϕ over a given encoding duration T_G is expressed with respect to the ratio q as:

$$\phi = \frac{\gamma \cdot G_{\mathrm{MEG}} \cdot A \cdot T_G}{\pi} \cdot \frac{sin(\pi q)}{1 - q^2} \qquad [7.10]$$

In typical conditions, where the aim is to obtain echo times shorter than the mechanical period, T_G will have to be maximized to maintain as high a sensitivity as

possible. This kind of encoding can be exploited for simultaneously acquiring several multiples of the base mechanical frequency, by means of a transducer capable of generating arbitrary mechanical waveforms (Garteiser *et al.* 2013).

7.2.2. *Multidirectional encoding*

In order to retrieve the mechanical properties of anisotropic tissues, displacements induced along the three orthogonal spatial directions have to be measured. This can be done by sequentially applying the motion-encoding gradients along the three directions, at the expense of the acquisition time being multiplied by three. Klatt *et al.* (Klatt *et al.* 2013) have proposed a method that enables simultaneous acquisitions of the three spatial directions in the case of a mono-frequential shear wave.

The underlying principle consists in applying an encoding gradient first in phase with the wave and then with an increasing phase offset. In the case when a single period of a sinusoidal encoding gradient is employed with a frequency equal to the wave frequency, following equation [7.4], the encoded phase is given by:

$$\phi(t_0) = \frac{\gamma G_0 A}{2f}\vec{u}_G.\vec{u}_u cos(2\pi f t_0 + \theta) \quad [7.11]$$

The simultaneous application of gradients along the three spatial directions (i = 1, 2, and 3, for the directions x, y, and z, respectively) with different initial execution times $t_{0i,n}$ (and thus different phase offsets) and a sampling of at least eight phases (N = 8) described by:

$$\Delta t_i = \frac{i}{N.f}$$
$$t_{0i,n} = n\,\Delta t_i, n = 0,1,\dots,N-1 \quad [7.12]$$

results in the nth encoded phase being the sum of the encoding obtained from the three gradients:

$$\phi_n = \sum_{i=1}^{3} \frac{\gamma G_{0,i} A}{2f}\vec{u}_{G,i}.\vec{u}_u \; cos\left(2\pi \frac{i.n}{N} + \theta_i\right) \quad [7.13]$$

In these conditions, equation [7.13] shows that the phase encoding of each direction translates into a different apparent frequency in the temporal evolution of ϕ_n. The encoding of x, y, and z directions is obtained by applying the Fourier transform and by retrieving first, second, and third harmonics, respectively. This method, called SLIM-MRE (SampLe Interval Modulation), has another version where the initial phase of the encoding is changed (Kearney *et al.* 2017).

7.2.3. *Diffusion MRE*

Due to the common requirement of applying encoding gradients, the elastography and diffusion techniques are similar in terms of acquisition methods. In fact, similar to diffusion-encoding gradients employed in diffusion-weighted sequences, the motion-encoding gradients used in MRE introduce a dephasing, with a greater effect in more mobile water molecules. The decrease in signal amplitude detected in such a way can be exploited to estimate the apparent or average diffusion coefficient via the methods described originally by Stejskal and Tanner (see chapter 4). The feasibility of this approach has been established in a phantom (Yin *et al.* 2014) and in a mouse brain (Yin *et al.* 2017b). The simultaneous encoding of incoherent motion related to diffusion in the image magnitude and periodic motion related to the acoustic wave in the phase image leads to an advantageous reduction of the acquisition time, compared to a consecutive execution of a diffusion scan and an MRE scan. Besides, spatial co-registration between elastography and diffusion data is automatic in the simultaneous approach. On the downside, undesired interactions between the two modalities can often occur when the wave amplitude reaches sufficiently high levels to affect the magnitude image due to intravoxel phase dispersion (Glaser *et al.* 2003).

7.2.4. *Optimal control MRE*

Most motion-encoding techniques for MRE are based on motion-encoding gradients. However, it is also possible to encode motion during the generation of the transverse magnetization. For this purpose, a gradient has to be applied, which can be constant (and not oscillating) while the excitation pulse selects the slice and encodes the motion into the phase of the signal. Computing such a pulse is not trivial and is achieved using optimal control.

Optimal control is a method that determines a control that has to be applied to bring a dynamic system from an initial state to a final state for a given optimality criterion defined via a cost function. From a mathematical point of view, this method is based on Pontryagin's maximum principle (Pontryagin *et al.* 1963). An analytical solution can be found in the case of low-dimensional problems, while in other cases it requires numerical solvers (Khaneja *et al.* 2005). In NMR and MRI, the dynamic system is composed of different isochromats[1] that have to be controlled and whose evolution can be described by Bloch equations (or by using quantum formulations). The applied control, whose duration has to be specified beforehand, is done by the RF pulse, which brings the dynamic system from an initial state, that in this case corresponds to the

1. An isochromat is defined as an ensemble of nuclear spins that are exposed to the same static magnetic field and behave in a similar way.

thermodynamic equilibrium state, to a target state, whose formulation below provides phase encoding similarly to the one obtained in MRE with an oscillating gradient:

$$\vec{M}_i^{\perp} = M_0 \begin{bmatrix} \cos\left(\pi . cos\left(\dfrac{2\pi(i-1)}{N_{iso}}\right)\right) \\ \sin\left(\pi . cos\left(\dfrac{2\pi(i-1)}{N_{iso}}\right)\right) \end{bmatrix} \quad [7.14]$$

$i \in [1\ ;\ N_{iso}]$ where N_{iso} represents the number of isochromats to be controlled along a wavelength as illustrated in figure 7.5 (N_{iso} = 10). The target state regards only the transverse magnetization, whose two components defined by equation [7.14] provide the desired phase of the MRI signal while targeting a maximized modulus of the transverse magnetization and, hence, maximized signal amplitude.

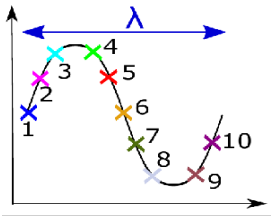

Figure 7.5. *Discretization of the wavelength for N_{iso} = 10 isochromats*

In order to calculate the RF field to be applied, the controlled system has to be described as precisely as possible. This is done using Bloch equations (by taking into account the relaxation time constants T_1 and T_2 during the execution of the RF pulse) and including the effect of a constant gradient applied while the shear wave is propagating. For the system described in figure 7.2, to obtain a slice in the *yOx* plane, a constant gradient will have to be applied along the z-direction. Displacement generated by the wave (equation [7.5]) leads in such cases to a variation of the B_0 field, given by:

$$\Delta B_0(y,z,t) = G_z\left(z + A.\sin\left(\omega t - \frac{2\pi . y}{\lambda}\right)\right) \quad [7.15]$$

where z represents the position in the direction of application of the constant gradient. In the case of 2D imaging, the fact that the isochromats have a resting position (in the absence of a shear wave) different from z = 0 has to be taken into account. Equation [7.15] describes the variation of the B_0 field that would be perceived by an isochromat at position z due to the simultaneous application of the G_z gradient and shear wave. A slice with a thickness Δz_{in} will correspond to a bandwidth (in Hz):

$$BW_{in} = \gamma G_z . \Delta z_{in} \quad [7.16]$$

Thus, for the optimization problem and the associated cost function, a certain number of isochromats within the desired slice has to be defined. This number has to be sufficiently large for the applied control to be robust such that the isochromats located within the control intervals follow the same dynamics as the controlled ones. However, a large number would considerably increase the computation time and the risk of the algorithm's non-convergence. Moreover, the spatial selectivity of the pulse has to be ensured by guaranteeing that the executed pulse does not affect the isochromats outside the selected slice. This is achieved by considering a certain number of isochromats located outside the slice thickness that should remain in the thermal equilibrium state. If Δz_{out} is the spatial location of these isochromats, this condition can be written as:

$$\vec{M_j} = \begin{pmatrix} 0 \\ 0 \\ M_0 \end{pmatrix}, \forall j | Z_j \in \Delta z_{out} \quad [7.17]$$

Figure 7.6 represents the magnitude of such a pulse (the phase is set to 0). It can be noticed that the magnitude has an upper bound of 94 µT, which corresponds to one of the optimization criteria that have to be defined beforehand to comply with the specifications of the employed transmit coil.

This MRE acquisition method presents advantages and disadvantages which should be mentioned. The advantages include a better signal-to-noise ratio for a given phase encoding efficiency (Van Reeth *et al.* 2018), the use of a constant, and not oscillating, gradient, which reduces the requirements regarding the gradients system, the possibility of acquiring signals with extremely short echo times and thus to target tissues with a short T_2, and the possibility of creating pulses that simultaneously encode several frequencies (Sango *et al.* 2020). The main constraints consist in the current impossibility of encoding displacements in other directions than the slice selection, the specific absorption rates considerations, since the executed pulses are more efficient when their amplitudes are higher, the need for precise knowledge of the experimental system (gradient amplitude, motion frequency, relaxation times T_2), although it is possible to take into account possible non-uniformities of B_0, and, finally, the computation time which can be rather long (in the order of several days) without a guarantee of satisfactory convergence. However, once the pulse is calculated, it can be used without any constraint whenever the experimental conditions correspond to the optimization criteria used in the optimization process.

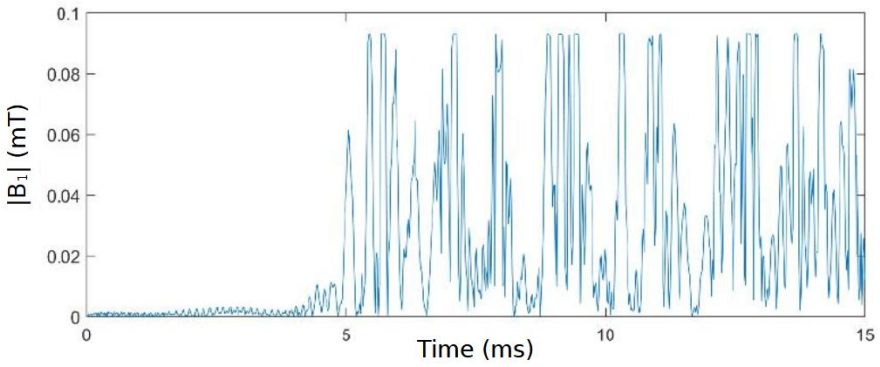

Figure 7.6. *Example of the magnitude (the phase is set to 0) of a pulse calculated via optimal control for MRE*

7.3. Main targeted organs and applications

7.3.1. *Liver MRE*

The liver is a preferential MRE target. Respiratory motion is a challenge, but it can be mitigated via breath-hold acquisitions. As it is located relatively close to the body surface, transmitting acoustic waves within its volume from one or two external sources is simple. Moreover, specific coils and long-established MRI scans are widely available and common in imaging centers. Finally, the measurement of the hepatic mechanical properties can be of great interest to several clinical diagnostic approaches.

Most of all, liver MRE has been used for the diagnosis of fibrosis. In this pathological condition, which can have viral (in particular, hepatitis B and C), alcoholic, or metabolic causes (non-alcoholic hepatic diseases such as non-alcoholic steatohepatitis), the presence of even small quantities of collagen fibers, whose stiffness is several orders of magnitude greater than a healthy liver's stiffness, leads to a significant increase in measured mechanical properties, even at earlier disease stages. Since the mechanical properties increase with the fibrosis degree, as illustrated in figure 7.7, threshold stiffness values can be determined to stage the patients' fibrosis class before resorting to the biopsy, which is the universally recognized reference method in clinical practice. The latter, although it is the only acknowledged technique for fibrosis diagnostics, is associated with low intraobserver repeatability, a very small analyzed volume that can lead to sampling biases, and a non-zero risk of complications for the patient. Besides, it is not well suitable for repeated examinations required for monitoring or therapeutic follow-up.

Several studies have quantified in detail the performance of MRE for the diagnostics of fibrosis. This technique is now considered to be a useful exam for fibrosis diagnostics in patients with non-alcoholic hepatic diseases (Chalasani *et al.* 2018) and the viscoelastic parameters of biomarkers have been validated in this context. Although inflammation that accompanies fibrosis can lead to greater mechanical properties, this increase is not sufficient to exploit stiffness as a clear inflammation marker. Other parameters obtained via MRE are being evaluated regarding their sensitivity to inflammation or other associated disorders such as ballooning. The viscoelastic ratio (Yin *et al.* 2017a), could eventually provide indications regarding these other hepatic diseases. Some works also measure the mechanical properties at several mechanical excitation frequencies, either to make the measurement more robust (Tzschätzsch *et al.* 2016), or to use the frequency dispersion coefficients as additional biomarkers (Asbach *et al.* 2010).

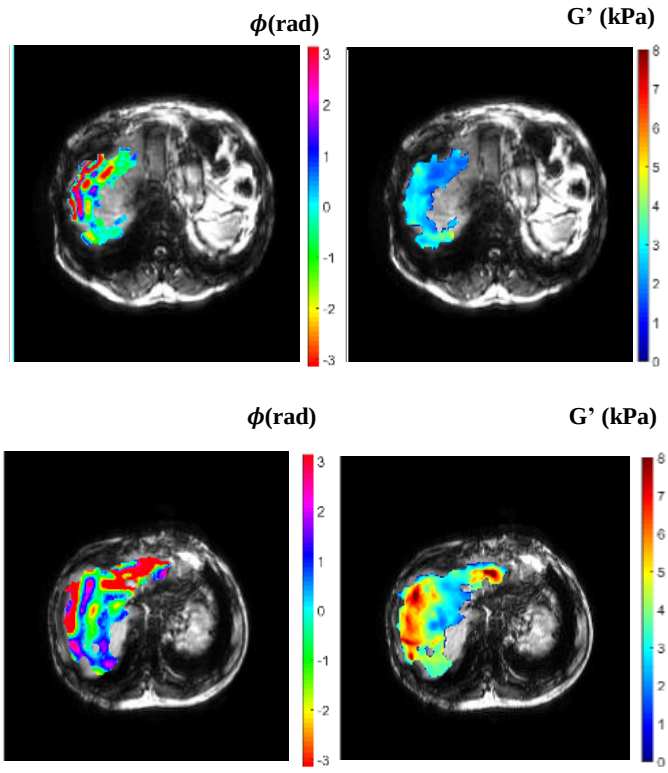

Figure 7.7. *Illustration of the MRE in the context of hepatic fibrosis. a) and b) Phase images illustrating the wave propagation and maps of the shear modulus (average: 2.4 ± 0.5 kPa), respectively, for a patient without fibrosis (METAVIR score F0). c) and d)*

Phase images illustrating the wave propagation and maps of the shear modulus (average: 4.4 ± 1.4 kPa), respectively, for a patient diagnosed with stage-F3 fibrosis.

In its more advanced form, fibrosis can worsen into cirrhosis, the most severe fibrosis stage in pathological classifications. In cirrhosis, the amount of collagen is very large for any degree of severity, but in some patients, this pathology is accompanied by more or less high hypertension in the hepatic and abdominal vascular systems, such as in the spleen. This hypertension progresses into esophagus varicose veins with a risk of bleeding. For cirrhosis patients, MRE can be performed both in the liver and spleen to evaluate portal hypertension due to the relationship between the vascular pressure in these two abdominal organs and their mechanical properties (Ronot *et al.* 2014).

MRE is also suitable for the mechanical characterization of cancerous hepatic lesions. The different tumor types encountered in the liver can differ in extracellular matrix composition, vascularization implications, or degree of cellularity and necrosis. However, in the context of cancerous lesions, precaution is required concerning MRE. In fact, the application of spatial filters, or the calculation of spatial derivatives required for most reconstructions can negatively affect the images via a point-spread function whose width can be similar to the lesion size. This problem is naturally exacerbated in the case of small tumors, i.e. smaller than 8 mm (Bohte *et al.* 2013).

7.3.2. *Brain MRE*

MRE of the brain is particularly interesting in the sense that assessing this organ via ultrasound elastography methods is very difficult due to the attenuation of the ultrasound in the skull. Several studies have investigated different pathologies and their effect on the elasticity of cerebral tissue measured via MRE.

7.3.2.1. *MRE and neuro-oncology*

About a dozen studies have performed MRE on different types of brain tumors (Bunevicius *et al.* 2020). Overall, glioblastomas have been reported as being softer than healthy parenchyma (Streitberger *et al.* 2014) and the elastic modulus of gliomas seems to decrease with increasing glioma grade. The elastic modulus of meningiomas seems to be more variable and heterogeneous than in other tumors. Globally, the discrimination of different tumor types using the elasticity parameter is restricted and it can hardly be sufficient for diagnosis, although it represents complementary information in addition to other MRI acquisitions.

7.3.2.2. *MRE and pathologies affecting the global elasticity of brain tissue*

Overall, neurodegenerative diseases are correlated with a decrease in the elastic modulus. Alzheimer's and Parkinson's diseases and dementia with Lewy bodies seem to lead to a significantly decreased stiffness of cerebral tissue (ElSheikh *et al.* 2017).

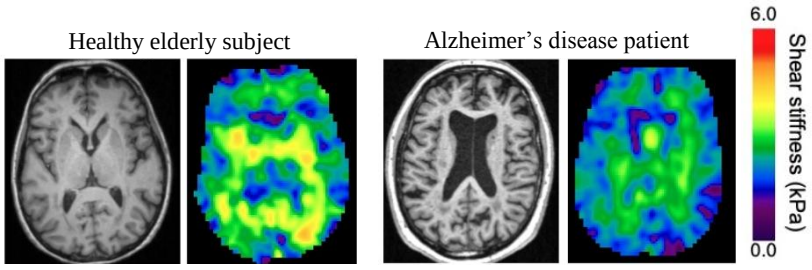

Figure 7.8. *Illustration of MRE of the brain in Alzheimer's disease. a), c) Anatomical images, b), d) maps of the shear modulus*

In a similar way, multiple sclerosis tend to induce a decrease in elastic modulus of cerebral tissue (Wuerfel *et al.* 2010) and the viscoelastic parameters seem capable of predicting the progression of this disease (Streitberger *et al.* 2012).

7.3.2.3. *MRE and pre-operatory planning in neurosurgery*

It is important to underline that the mechanical properties of cerebral tissue are also very important for pre-operatory planning. In particular, the adherence of the tumor to the surrounding tissue represents valuable information that can help neurosurgeons plan a resection procedure. Discontinuities of displacement fields measured by MRE have been proposed as markers for predicting this adherence, with a good correlation with the adherence estimated during interventions on meningiomas and vestibular schwannomas (Yin *et al.* 2017c).

7.3.3. *MRE and other organs*

Several other organs are worth to be investigated using MRE. However, the fact that this is not currently the case is essentially related to the intrinsic difficulties in applying MRE to these organs. Such challenges are related to the design of the mechanical wave-generating device and its validation for clinical use, the MRI data acquisition required for the elastogram reconstruction, or the reconstruction of elastograms in tissues where the usual hypotheses (isotropy, local homogeneity) are not valid. The three examples below illustrate such cases.

7.3.3.1. *MRE of the breast*

Breast cancer is the most common cancer in females and its screening methods either are invasive in the case of biopsies or ionizing modalities in the case of mammographies. Therefore, there is a great need for alternative detection and staging, all the more so as mortality is mostly due to the resulting metastases rather than primary tumors. MRI is not a primary tool for breast cancer screening. Breast MRI scans require a prone position of the patient with a dedicated multichannel receive coil surrounding each breast. The wave-generating device has then to be integrated into the receive coil, which excludes any large or stand-alone device. Some research groups have developed functional solutions that provide images with good quality (Plewes *et al.* 2000; Sinkus *et al.* 2005). An MRE exam has to be performed covering the entire breast and with a sufficient spatial resolution for precise demarcation of tumor areas. Currently, this can be done in slightly more than ten minutes, which, although promising, is still too long to be included in a clinical protocol. To this day, in terms of results, the shear modulus obtained via MRE alone does not allow tumor staging and detection of lesions with the highest probability of metastasis. However, the retrieved information is valuable and complementary to that obtained via other imaging methods (in particular, with contrast-agent dynamic MRI). A detailed and recent review of MRE applications for breast cancer screening has been compiled by Bohte *et al.* (Bohte *et al.* 2018).

7.3.3.2. *MRE of the muscles*

Since the muscles are organized into fiber fascicles, at a local scale, they exhibit properties of transverse isotropy and not three-dimensional isotropy, which is an assumption required for many reconstruction algorithms and for LFE in particular (see section 7.1.3.2). A transversely isotropic medium is characterized by two shear moduli, which in the case of muscles correspond to the parallel and transverse orientation with respect to the fiber direction. Characterizing these two moduli requires *a priori* knowledge of the fiber orientation, which can be obtained via diffusion MRI. However, few studies has been published so far in this direction, and researchers have mostly made different choices ranging from simplified hypotheses of isotropic medium to mono-directional mechanical excitations or spatial filtering to isolate a single wave component.

In terms of devices, most studies have used a pneumatic or electromechanical transducer with a surface coil placed as close as possible to the investigated muscles. The latter are essentially muscles of the thigh and calf or biceps muscles. The results (Dresner *et al.* 2001) show a growing linear correlation between the muscular contractions for different applied loads and the shear modulus representing the muscular stiffness. These stiffness variations between resting and contraction states are the basis for extracting parameters to characterize muscular disorders, especially in the case of Duchenne muscular dystrophy (Bensamoun *et al.* 2015).

7.3.3.3. *MRE of the heart*

Cardiovascular diseases are the first cause of death in Western countries and their early detection is of major importance. Characterizing the myocardium contractility is fundamental in many cardiac pathologies and MRE is quite relevant in this case since the shear modulus could be directly related to the intracardiac pressure (Elgeti *et al.* 2008). However, MRE of the heart presents several specific aspects that strongly hinder its exploration. The main difficulties are: (1) the heart is a muscle with a myocardium fiber architecture that is even more complex than the one in skeletal muscles; (2) the biomechanical properties of the myocardium have to be characterized at different instants of the cardiac cycle which implies a constraining synchronization of the acquisitions, especially arrhythmias are present in some pathologies, hence leading to long and repeated scans; (3) the heart is located within the thoracic cage and surrounded by other organs. Consequently, transmitting a shear wave using an external device is not simple. Most of the performed studies have employed very low excitation frequencies.

7.3.4. *Other applications*

As illustrated before, MRE has been mainly developed for diagnostic applications. However, the versatility of this technique offers several opportunities that extend beyond such an objective. Here, we shall illustrate two particularly novel applications: on the one hand, MRE as a biomechanical characterization method and, on the other hand, MRE as a guidance method for thermal ablations in interventional MRI.

7.3.4.1. *MRE as a biomechanical characterization tool*

Knowing the mechanical behavior of biological tissue is fundamental in many research and engineering fields. This knowledge is mainly based on experimental results obtained *in vitro* for reasons that are related to experimental protocols. This is a real limitation in the sense that the biomechanical behavior of tissues can exhibit significant differences between the living and *post-mortem* states. In general, elastography methods have the theoretical potential of characterizing the mechanical properties of tissues in their normal condition *in vivo*. However, they have not been originally developed for the purpose of quantitative biomechanical characterization. Our goal here is to illustrate how the MRE technique can be adapted to this particularly original objective.

Diagnostic elastography is essentially based on the hypothesis of purely elastic linear behavior. Clearly, the biomechanical behavior of tissues is much more complex: biological tissue can typically be viscoelastic, with a non-linear and anisotropic behavior, among other properties. Some of these properties can be characterized via MRE methods.

Viscoelastic properties have historically been the first ones to be investigated. Since the early 2000s, some methods for inverting the wave equation have been adapted to

characterize not only the elasticity but also the viscosity of biological tissues, essentially for diagnostic purposes. One of the goals of these studies was to investigate biomarkers other than just elasticity and to quantify their sensitivity to some pathologies (Sinkus *et al.* 2005). In a viscoelastic medium, the shear modulus G is complex and equation [7.2] can be rewritten by simply decomposing G into a real part and an imaginary part: $G = G' + iG''$. G′ is called storage modulus and represents purely elastic behavior. G″ is called loss modulus and represents the viscous behavior of tissue. This representation in terms of G′, G″, and their frequency dependence are very common in biomechanics and rheology for viscoelastic characterizations. By inverting the wave equation with the hypothesis of a complex wave number, it is thus possible to characterize G′ and G″ as well as their dynamic behavior, for example using different mechanical excitation frequencies. This approach has been applied to different organs to model them with different rheological models (Guo *et al.* 2012; Testu *et al.* 2017). This kind of novel data represents a major contribution in the field of biomechanics. As an example, until the 2000s, there was a considerable variation in the viscoelastic properties of brain tissue reported in the literature, spanning a range of two orders of magnitude (Chatelin *et al.* 2010). This variation was mainly due to the specificity of *in vitro* protocols. For the first time, MRE allowed the viscoelastic behavior of *in vivo* brain tissue to be established in its normal state (Sack *et al.* 2008; Vappou *et al.* 2008).

In addition to their viscoelastic behavior, some tissues have a strong mechanical anisotropy. This is the case of tissues in muscles or the brain. MRE is particularly suitable for characterizing this anisotropy due to the possibility of encoding the three displacement components with the same quality and precision. From an experimental point of view, this approach is rather powerful as it provides an *in vivo* characterization whereas an *in vitro* measurement requires sample preparation, for example by cutting the sample along different directions before characterizing them. Finally, we can also mention the characterization of the poroelastic properties of tissues (Perriñez *et al.* 2010). This behavior is characterized by the presence of a liquid phase within a solid matrix. When subjected to deformation, the fluid circulation and its interaction with the solid phase give the tissue a certain resistance, which is particularly difficult to characterize *in vitro*. Once again, MRE has overcome this major barrier for applications in organs such as the brain (Weaver *et al.* 2012).

Beyond the contribution of these methods to biomechanics, using more complex models than a simple linear elastic model carries also diagnostic opportunities in terms of novel biomarker propositions, which are currently employed in several clinical studies as mentioned throughout section 7.3.

7.3.4.2. *MRE for thermal therapy monitoring*

In this section, we describe how MRE can aid in monitoring thermal therapies. Although it is certainly a minor application, this example helps illustrate how some methodological MRE adaptations can unlock novel applications.

Minimally invasive thermal ablations emerged in the last decades as a safe, efficient, and less complicated alternative to traditional surgery in numerous applications. The safety and efficiency of these therapies are, nevertheless, based on real-time guidance and monitoring via medical imaging modalities. Among the latter, MRI offers several advantages, such as intrinsic contrast in soft tissues and the possibility of monitoring the temperature in real time via MR thermometry. However, one of the major challenges in this field consists in obtaining new biomarkers that are sensitive and specific to the structural integrity of the tissue during its ablation. In theory, the mechanical properties of tissues can play this role, as has been shown in some studies that used ultrasound elastography for monitoring thermal ablations (Mariani *et al.* 2014). Some MRE studies have also found differences between elasticity before and after thermal ablation (Chen *et al.* 2014). Nonetheless, traditional MRE techniques are still unsuitable for real-time monitoring due to the associated acquisition times. In this context, several research teams have sought to adapt MRE to the interventional context, in particular, to obtain biomechanical information in a real-time fashion for monitoring ablations. Corbin *et al.* (Corbin *et al.* 2016) have developed a percutaneous interventional MRE method based, on the one hand, on direct wave generation by means of the interventional needle, without resorting to an additional external transducer, and, on the other hand, on a fast acquisition/reconstruction method (fractional encoding, phase steps number reduced to 3, sliding window) providing elastograms at a timescale of seconds. In addition, without additional acquisitions, this method estimates the temperature via PRFS (Proton Resonance Frequency Shift) thermometry. For this purpose, two acquisitions are performed using MEGs with opposite polarities. The difference between these two images helps to retrieve the contribution of the displacements due to the wave propagation, whereas, on the contrary, the sum of these 2 images helps to detect the changes of phase due to temperature variations.

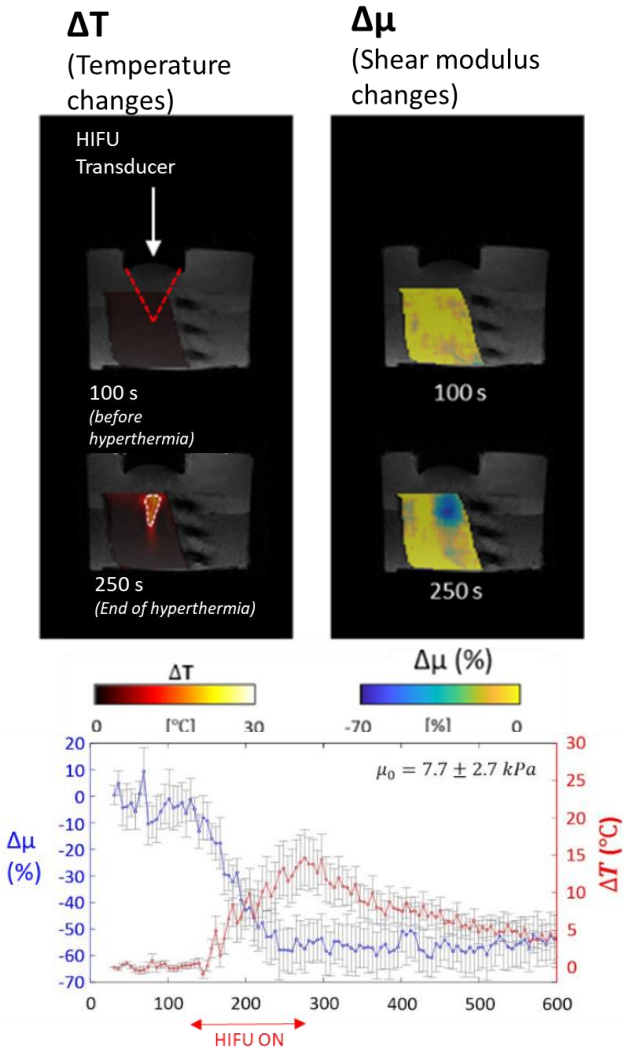

Figure 7.9. *Illustration of MRE for monitoring hyperthermia induced by high-intensity focused ultrasound (HIFU) using simultaneous elastography and thermometry in swine muscle in vitro. Here, moderate hyperthermia (~ 15 °C) is associated with a considerable and permanent decrease in shear modulus.*

Other methods have been developed specifically for monitoring thermal ablations via high-intensity focused ultrasound (HIFU). In this case, displacements are produced directly by the ultrasound transducer by means of the acoustic radiation force, which makes an additional external transducer unnecessary (Souchon *et al.* 2008; Vappou *et al.* 2018).

7.4. Conclusion

MRE is a multidisciplinary technique. Above all else, it requires the generation of shear waves within the tissue to be investigated and, thus, appropriate devices have to be developed and optimized for the targeted application. Being an MRI technique in its own right, it requires good knowledge of magnetic resonance physics concepts. The reconstruction of maps can mean solving a complex inverse problem, all the more so as MRE is turning to applications in organs with more complex geometry and structure than the originally considered liver. Regarding this topic, some research groups have made their reconstruction software available:

1) LFE by the Mayo Clinic in Rochester (United States): www.mayo.edu/research/labs/advanced-medical-imaging-technology/focus-areas;

2) MDEV (an inversion algorithm for multifrequency wave equations) by the Charité in Berlin (Germany): https://bioqic.de/bioqic-server/.

In terms of clinical applications, the contribution of MRE in the diagnostics of hepatic fibrosis is undeniable. In about twenty years, it has become a renowned method for a global examination of the organ, which cannot be done using the reference biopsy method. Another clinical application that attracts many efforts is the brain. Here, again, no other modality can provide measurements of the mechanical properties with such a large coverage. However, research is ongoing to bring brain MRE to the same level as liver MRE, either by focusing on the generation and transmission of waves inside the brain or on the reconstruction of the mechanical properties of the brain. The wide scope of research in this domain is supported by the growing number of scientific articles of the last twenty years, which have seen MRE transitioning from the stage of a novel MRI technique to the stage of a well-established diagnostic modality in clinical routine.

7.5. Acknowledgments

The authors are deeply thankful to Lucie Hiscox for the provided clinical illustrations of brain MRE.

7.6. Bibliography

Asbach, P., Klatt, D., Schlosser, B., Biermer, M., Muche, M., Rieger, A., Loddenkemper, C., Somasundaram, R., Berg, T., Hamm, B., Braun, J., Sack, I. (2010). Viscoelasticity-based Staging of Hepatic Fibrosis with Multifrequency MR Elastography. *Radio-logy*, 257(1), 80–86.

Bensamoun, S.F., Charleux, F., Debernard, L., Themar-Noel, C., Voit, T. (2015). Elastic properties of skeletal muscle and subcutaneous tissues in Duchenne muscular dystrophy by magnetic resonance elastography (MRE): A feasibility study. *IRBM*, 36(1), 4–9.

Bohte, A.E., Garteiser, P., De Niet, A., Groot, P.F., Sinkus, R., Stoker, J., Nederveen, A.J. (2013). MR elastography of the liver: defining thresholds for detecting viscoelastic changes. *Radiology*, 269(3), 768–776.

Bohte, A.E., Nelissen, J.L., Runge, J.H., Holub, O., Lambert, S.A., of Graaf, L., Kolkman, S., van der Meij, S., Stoker, J., Strijkers, G.J., Nederveen, A.J., Sinkus, R. (2018). Breast magnetic resonance elastography: a review of clinical work and future perspectives. *NMR Biomed.*, 31(10), e3929.

Bunevicius, A., Schregel, K., Sinkus, R., Golby, A., Patz, S. (2020). Review: MR elastography of brain tumors. *NeuroImage Clin.*, 25, 102109.

Chalasani, N., Younossi, Z., Lavine, J.E., Charlton, M., Cusi, K., Rinella, M., Harrison, S.A., Brunt, E.M., Sanyal, A.J. (2018). The diagnosis and management of nonalcoholic fatty liver disease: Practice guidance from the American Association for the Study of Liver Diseases. *Hepatology*, 67(1), 328–357.

Chatelin, S., Constantinesco, A., Willinger, R. (2010). Fifty years of brain tissue mechanical testing: from in vitro to in vivo investigations. *Biorheology*, 47(5/6), 255–276.

Chen, J., Woodrum, D.A., Glaser, K.J., Murphy, M.C., Gorny, K., Ehman, R. (2014). Assessment of in vivo laser ablation using MR elastography with an inertial driver. *Magn. Reson. Med.*, 72, 59–67.

Corbin, N., Vappou, J., Breton, E., Boehler, Q., Barbé, L., Renaud, P., de Mathelin, M. (2016). Interventional MR elastography for MRI-guided percutaneous procedures. *Magn. Reson. Med.*, 75, 1110–1118.

Dresner, M.A., Rose, G.H., Rossman, P.J., Muthupillai, R., Manduca, A., Ehman, R.L. (2001). Magnetic resonance elastography of skeletal muscle. *J. Magn. Reson. Imaging*, 13(2), 269–276.

Elgeti, T., Rump, J., Hamhaber, U., Papazoglou, S., Hamm, B., Braun, J., Sack, I. (2008). Cardiac magnetic resonance elastography: initial results. *Investigative Radiology*, 43(11), 762–772.

Elsheikh, M., Arani, A., Perry, A., Boeve, B.F., Meyer, F.B., Savica, R., Ehman, R.L., Huston, J., III (2017). MR Elastography Demonstrates Unique Regional Brain Stiffness Patterns in Dementias. *AJR Am J Roentgenol.*, 209(2), 403–408.

Garteiser, P., Sahebjavaher, R.S., Ter Beek, L.C., Salcudean, S., Vilgrain, V., Van Beers, B.E., Sinkus, R. (2013). Rapid acquisition of multifrequency, multislice and multidirectional MR elastography data with a fractionally encoded gradient echo sequence. *NMR Biomed.*, 26(10), 1326–1335.

Glaser, K.J., Felmlee, J.P., Manduca, A., Ehman, R.L. (2003). Shear stiffness estimation using intravoxel phase dispersion in magnetic resonance elastography. *Magn. Reson. Med.*, 50, 1256–1265.

Guo, J., Posnansky, O., Hirsch, S., Scheel, M., Taupitz, M., Braun, J., Sack, I. (2012). Fractal network dimension and viscoelastic powerlaw behavior: II. An experimental study of structure-mimicking phantoms by magnetic resonance elastography. *Phys. Med. Biol.*, 57(12), 4041–4053.

Kearney, S.P., Majumdar, S., Royston, T., Klatt, D. (2017). Simultaneous 3D MR elastography of the in vivo mouse brain. *Phys. Med. Biol.*, 62(19), 7682–7693.

Khaneja, N., Reiss, T., Kehlet, C., Schulte-Herbrüggen, T., Glaser, S.J. (2005). Optimal control of coupled spin dynamics: design of NMR pulse sequences by gradient ascent algorithms. *J. Magn. Reson.*, 172(2), 296–305.

Klatt, D., Yasar, T.K., Royston, T.J., Magin, R.L. (2013). Sample interval modulation for the simultaneous acquisition of displacement vector data in magnetic resonance elastography: theory and application. *Phys. Med. Biol.*, 58(24), 8663–8675.

Knutsson, H., Westin, C.F., Granlund, G. (1994). Local multiscale frequency and bandwidth estimation. *Proceedings. ICIP-94*, 1, 36–40.

Lewa, C.J. (1991). Magnetic resonance imaging in the presence of mechanical waves. *Spectroscopy Letters*, 24(1), 55–67.

Manduca, A., Lake, D.S., Kruse, S.A., Ehman, R.L. (2003). Spatio-temporal directional filtering for improved inversion of MR elastography images. *Med. Image Anal*, 7(4), 465–473.

Mariani, A., Kwiecinski, W., Pernot, M., Balvay, D., Tanter, M., Clement, O., Cuenod, C.A., Zinzindohoue, F. (2014). Real time shear waves elastography monitoring of thermal ablation: in vivo evaluation in pig livers. *J. Surg. Res.*, 188(1), 37–43.

Murphy, M.C., Huston, J., III, Jack, C.R. Jr., Glaser, K.J., Manduca, A., Felmlee, J.P., Ehman, R.L. (2011). Decreased brain stiffness in Alzheimer's disease determined by magnetic resonance elastography. *J. Magn. Reson. Imaging*, 34, 494–498.

Muthupillai, R., Lomas, D.J., Rossman, P.J., Greenleaf, J.F., Manduca, A., Ehman, R.L. (1995). Magnetic resonance elastography by direct visualization of propagating acoustic strain waves. *Science*, 269(5232), 1854–1857.

Perriñez, P.R., Kennedy, F.E., Van Houten, E.E.W., Weaver, J.B., Paulsen, K.D. (2010). Magnetic resonance poroelastography: An algorithm for estimating the mechanical properties of fluid-saturated soft tissues. *IEEE Transactions on Medical Imaging*, 29(3), 746–755.

Plewes, D.B, Bishop, J., Samani, A., Sciarretta, J. (2000). Visualization and quantification of breast cancer biomechanical properties with magnetic resonance elastography. *Phys. Med. Biol.*, 45(6), 1591–1610.

Pontryagin, L.S., Boltyanskii, V.G., Gamkrelidze, R.V., Mishechenko, E.F. (1963). The Mathematical Theory of Optimal Processes. *Journal of Applied Mathematics and Mechanics*, 43(10/11), 514–515.

Ronot, M., Lambert, S., Elkrief, L., Doblas, S., Rautou, P.E., Castera, L., Vilgrain, V., Sinkus, R., Van Beers, B.E., Garteiser, P. (2014). Assessment of portal hypertension and high-risk oesophageal varices with liver and spleen three-dimensional multifrequency MR elastography in liver cirrhosis. *Eur. Radiol.*, 24(6), 1394–1402.

Runge, J.H., Hoelzl, S.H., Sudakova, J., Dokumaci, A.S., Nelissen, J.L., Guenthner, C., Lee, J., Troelstra, M., Fovargue, D., Stoker, J., Nederveen, A.J., Nordsletten, D., Sinkus, R. (2019). A novel magnetic resonance elastography transducer concept based on a rotational eccentric mass: preliminary experiences with the gravitational transducer. *Phys. Med. Biol.*, 64(4), 045007.

Sack, I., Beierbach, B., Hamhaber, U., Klatt, D., Braun, J. (2008). Non-invasive measurement of brain viscoelasticity using magnetic resonance elastography. *NMR Biomed.*, 21, 265–271.

Sango Solanas P., Tse Ve Koon K., Van Reeth E., Ratiney H., Millioz F., Caussy C., Beuf O. (2022). Short echo time dual-frequency MR Elastography with Optimal Control RF pulses. *Scientific Reports*. 12, Article number: 1406.

Sinkus, R., Tanter, M., Xydeas, T., Catheline, S., Bercoff, J., Fink, M. (2005). Viscoelastic shear properties of in vivo breast lesions measured by MR elastography. *Magn. Reson. Imaging.*, 23(2),159–165.

Souchon, R., Salomir, R., Beuf, O., Milot, L., Grenier, D., Lyonnet, D., Chapelon, J.Y., Rouvière, O. (2008). Transient MR elastography (t-MRE) using ultrasound radiation force: theory, safety, and initial experiments in vitro. *Magn. Reson. Med.*, 60(4), 871–881.

Streitberger, K.J., Sack, J., Krefting, D., Pfüller, C., Braun, J., Paul, F., Wuerfel, J. (2012). Brain Viscoelasticity Alteration in Chronic-Progressive Multiple Sclerosis. *Plos one*, 7(1), e29888.

Streitberger, K.J., Reiss-Zimmermann, M., Freimann, F.B., Bayerl, S., Guo, J., Artl, F., Wuerfel, J., Braun, J., Hoffmann, K.T., Sack, I. (2014). High-Resolution Mechanical Imaging of Glioblastoma by Multifrequency Magnetic Resonance Elastography. *Plos one*, 9(10), e110588.

Testu, J., McGarry, M.D.J., Dittmann, F., Weaver, J.B., Paulsen, K.D., Sack, I., Van Houten, E.E.W. (2017). Viscoelastic power law parameters of in vivo human brain estimated by MR elastography. *J. Mech. Behav. Biomed. Mater.*, 74, 333–341.

Tse, Z.T.H., Janssen, H., Hamed, A., Ristic, M., Young, I., Lamperth, M. (2009). Magnetic resonance elastography hardware design: A survey. *Proc. Inst. Mech. Eng. H.*, 223(4), 497–514.

Tzschätzsch, H., Guo, J., Dittmann, F., Hirsch, S., Barnhill, E., Jöhrens, K., Braun, J., Sack, I. (2016). Tomoelastography by multifrequency wave number recovery from time-harmonic propagating shear waves. *Med. Image. Anal.*, 30, 1–10.

Van Houten, E.E.W, Paulsen, K.D., Miga, M.I., Kennedy, F.E., Weaver, J.B. (1999). An overlapping subzone technique for MR-based elastic property reconstruction. *Magn Reson Med.*, 42(4), 779–786.

Van Reeth, E., Lefebvre, P.M., Ratiney, H., Lambert, S.A., Tesch, M., Brusseau, E., Grenier, D., Beuf, O., Glaser, S.J., Sugny, D., Tse Ve Koon, K. (2018). Constant gradient elastography with optimal control RF pulses. *J. Magn. Reson.*, 294, 153–161.

Vappou, J., Breton, E., Choquet, P., Willinger, R., Constantinesco, A. (2008). Assessment of in vivo and post-mortem mechanical behavior of brain tissue using magnetic resonance elastography. *J. Biomech.*, 41(14), 2954–2959.

Vappou, J., Bour, P., Marquet, F., Ozenne, V., Quesson, B. (2018). MR-ARFI-based method for the quantitative measurement of tissue elasticity: application for monitoring HIFU therapy. *Phys. Med. Biol.*, 63(9), 095018.

Venkatesh, S.K., Yin, M., Ehman, R.L. (2013). Magnetic Resonance Elastography of Liver: Technique, Analysis and Clinical Applications. *J. Magn. Reson. Imaging.*, 37(3), 544–555.

Weaver, J.B., Pattison, A.J., McGarry, M.D., Perreard, I.M., Swienckowski, J.G., Eskey, C.J., Lollis, S.S., Paulsen, K.D. (2012). Brain mechanical property measurement using MRE with intrinsic activation. *Phys. Med. Biol.*, 57(22), 7275–7287.

Wuerfel, J., Paul, F., Beierbach, B., Hamhaber, U., Klatt, D., Papazoglou, S., Zipp, F., Martus, P., Braun, J., Sack, I. (2010). MR-elastography reveals degradation of tissue integrity in multiple sclerosis. *NeuroImage*, 49(3), 2520–2525.

Yin, Z., Magin, R.L., Klatt, D. (2014). Simultaneous MR elastography and diffusion acquisitions: Diffusion-MRE (dMRE). *Magn. Reson. Med.*, 71, 1682–1688.

Yin, M., Glaser, K.J, Manduca, A., Mounajjed, T., Malhi, H., Simonetto, D.A., Wang, R., Yang, L., Mao, S.A., Glorioso, J.M., Elgilani, F.M., Ward, C.J., Harris, P.C., Nyberg, S.L., Shah, V.H., Ehman, R.L. (2017a). Distinguishing between Hepatic Inflammation and Fibrosis with MR Elastography. *Radiology*, 284(3), 694–705.

Yin, Z., Kearney, S.P., Magin, R.L., Klatt, D. (2017b). Concurrent 3D acquisition of diffusion tensor imaging and magnetic resonance elastography displacement data (DTI-MRE): Theory and in vivo application. *Magn. Reson. Med.*, 77, 273–284

Yin, Z., Hughes, J.D., Glaser, K.J., Manduca, A., Van Gompel, J., Link, M.J., Romano, A., Ehman, R.L., Huston, J., III (2017c). Slip interface imaging based on MR-elastography preoperatively predicts meningioma–brain adhesion. *J. Magn. Reson. Ima-ging*, 46, 1007–1016.